Volume 16, Issue 4, 162527 (1-12)

International Journal of Nano Dimension (IJND)

https://dx.doi.org/10.57647/j.ijnd.2025.1604.27

Elucidating the structural, optical, and magnetic properties of tin-doped manganese Sulphide (TMS) nanomaterials

Jeyamalar Krishnasamy[1,*], Selvarajan Palanisamy[2], Vella Durai Subbaiah Chelladurai[3]

[1]*Research scholar, Department of Physics, Bharathiar University, Coimbatore-641046, Tamilnadu, India.*
[2]*Department of Physics, Aditanar College of Arts and Science, Tiruchendur-628216, Tamilnadu, India.*
[3]*PG and Research Department of Physics, Sri Paramakalyani College, Alwarkurichi, Tenkasi-627412, Tamilnadu, India.*

[*]**Corresponding author:** jeyamhanish@gmail.com

Original Research

Received:
11 February 2025
Revised:
28 April 2025
Accepted:
3 May 2025
Published online:
10 May 2025
Published in issue:
17 May 2025

Abstract:

Tin-doped Manganese Sulphide (TMS) was created by utilizing green synthesis with grape juice. The prepared TMS nanomaterial underwent examinations with the X-Ray Diffraction (XRD), UV-visible spectral (UV), Scanning Electron Microscope (SEM), Atomic Force Microscope (AFM), High Resolution Transmission Electron Microscope (HRTEM), Selected Area Electron Diffraction (SAED), Energy Dispersive Spectroscopic (EDS), and Vibrating Sample Magnetometer (VSM) techniques. The TMS material's structure was discovered by the XRD method to have a cubic structure, and the sample's particle size was calculated to be 22.651 nm. According to a SEM analysis, the sample contains particles that are somewhat agglomerated and have the shape of flowers. It has been determined from HRTEM and SAED tests that the nanoparticle is a single crystal. The EDS method was used to identify elements like Mn, S, and Sn. The band gap of TMS nanomaterial is estimated to be 3.42 eV by UV-visible spectral analysis and AFM investigation provides 2-d and 3-d pictures of the sample. According to VSM characterisation, TMS nanomaterial is a type of paramagnetic material. The results of research using FTIR, thermal, fluorescence, cyclic voltammetry, and impedance to characterize tin-doped MnS (TMS) nanomaterial are evaluated.

Keywords: Antibacterial activity; Impedance; Microscopy; MnS; Sn- doped; Spectroscopy; VSM

1. Introduction

In recent years, interest in nanocrystalline materials has grown due to the promise they offer for technological applications as well as the problems they bring to our knowledge of basic science. The peculiar and frequently advantageous features that nanocrystalline materials possess as a result of the advent of crystalline boundary-dominated physics when the crystalline size approaches roughly 100 nm and lower are the source of this interest. The nanocomposite synthesized via reduction agent shows uniform distribution and enhanced thermal stability. Crystalline grain boundaries are no longer considered to be planar defects at these incredibly small length scales since their volume is equivalent to the interior of the crystalline. Nanomaterials have a wide range of uses, including in solar cells, superplastic ceramics, nonlinear optics, optoelectronics, photonics, sensing, storage and processing adsorbents, catalysis, quantum electronics, nonlinear optics, and optoelectronics [1–4]. Semiconductor metal sulphide nanoparticles have been studied by numerous researchers, and they possess a number of unique properties that suggest potential applications in a variety of fields, including photo-catalysis, solar cells, display panels, and devices like single electron transistors, among others, Novel eco-friendly synthesis of pyranopyrimidinone and xanthene derivatives using ZnO-starch nanocomposite catalyst [5–7]. Alcohol oxidation is a crucial reaction in organic synthesis [8]. A semiconductor with potential applications, manganese sulphide (MnS) can be found in three forms: -MnS, -MnS, and -MnS [9, 10]. By heating a combination of sulphur and manganese chloride in oleyamine, Joo et al. published a study on MnS nanoparticles [11].

Puglisi et al. have created MnS nanomaterial by degrading manganese oleate and elemental sulphur [12]. Star-shaped MnS nanocrystals with a coercive field were made by Tian and his colleagues [13]. In recent years, composite nanomaterials have attracted a lot of attention due to the coupling of two semiconductor nanocrystals, which results in a number of unique optical and electrical features [14]. The formation of semiconductor nanocomposites, such as ZnS/CdS, CdS/HgS, ZnO/$LaMnO_3$, ZnO/SnO_2 and ZnS/CdSe, has been the subject of several studies [15–19]. Nanocomposites have shown promise in various applications. This research investigates the molecular stability and bonding mechanisms of doped nanoparticles using computational methods [20]. In this study, it is intended to manufacture tin-doped MnS nanomaterial by green method, taking into consideration the varied applications of undoped and doped semiconductor nanomaterials. The produced nanomaterials have undergone numerous characterization investigations, including FTIR, XRD, SEM, UV-visible spectral, and photoluminescence investigations. The results are discussed in this paper.

2. Experimental and methods

2.1 Synthesis of the sample by green method

MnS: Sn (TMS) nanoparticles were synthesized by the green synthesis, which is a simple and environmentally friendly method [21–23]. The precursor components included manganese acetate, tin chloride, and thiourea, which were all purchased from Merck India. In Tamilnadu, green grapes were purchased from a fruit stand. After washing and air-drying the grapes, green grape juice was extracted. In the sample preparation process, double distilled water was employed as the solvent. Aqueous saturated solutions of manganese acetate, thiourea, and tin chloride were combined with 15 mL of green grape juice in a 1:1:0.02 molar ratios. Using a hot-plate magnetic stirrer, this liquid was constantly swirled for three hours at 80 degrees Celsius. By adding a 1 M aqueous solution of sodium hydroxide, the pH of the solution was brought down to 10. The material developed a brown precipitate, which was then removed using high-quality filter paper. The generated sample was cleaned in double-distilled water and acetone before being dried at 35 °C. Fig. 1 shows an image of the prepared TMS nanomaterial. It can be noted that the sample has a little blackish-brown colour.

2.2 Instrumentations

The powder X-ray diffraction (XRD) pattern of the as-prepared sample was recorded using a Rigaku D/max-rB powder X-ray diffractometer with CuKα radiation (λ = 1.54178) at a scanning rate of 6 °C/min in the $20-80°$ range. The SEM image of the nano-powdered sample was captured using a Hitachi SEM S 2400 instrument. EDX measurements, typically attached to SEM equipment, were also performed. High-resolution images of the sample were obtained using a JEOL 3010 HRTEM with a UHR pole piece operating at an accelerating voltage of 300 kV in selected area electron diffraction (SAED) mode to analyze the TMS nanomaterial. The TMS nanomaterial was mixed with acetone and placed on a Si substrate for AFM analysis using a Nanosurf easy 2 scan instrument. The infrared spectrum of the sample was recorded in the $400-4000$ cm^{-1} range using a Shimadzu 8400S FT-IR spectrometer. The powder sample was finely dispersed in KBr using an agate mortar, well-ground, and then pressed into circular discs of approximately 10 mm diameter and 0.5 mm thickness at a pressure of 250 MPa. The pellet was dried with IR light before recording the FT-IR spectrum. The ultraviolet, visible, and infrared absorbance spectra of the TMS nanomaterial were captured using a Varian Cary 5E UV-Vis-NIR spectrophotometer. Impedance analysis was conducted using an IM 6 ZAHNER impedance analyzer from Germany. At IIT Madras, a VSM investigation was performed on the TMS nanomaterial. Cyclic voltammetric studies were carried out using a CH1650C electrochemical station. Thermal analysis was performed using a Hitachi STA7000. Fluorescence studies were analyzed with a Varian/Cary Eclipse/Winflr/Default: An FMSW instrument. Antimicrobial studies were conducted using the disc diffusion method.

Figure 1. The synthesized tin-doped MnS nanomaterial.

3. Results and discussion

3.1 Powder XRD studies

Fig. 2 displays the MnS: Sn nanomaterial's recorded XRD pattern. On the pattern, every diffraction peak was linked to a cubic unit cell and the reflection planes are assigned with Miller indices such as (111), (002), (200), (220), (311), (222), and (400). Since the reflection planes belong to the cubic system, the lattice parameter (a) of the sample has been calculated using the relation $a = d(h^2 + k^2 + l^2)^{1/2}$ where d is the interplanar spacing and h, k, l are the Miller indices of the crystal planes. The estimated value of lattice parameter of the tin-doped MnS sample is 5.2301 Å. It is noted that the recorded powder XRD pattern of TMS nanoparticles and the JCPDS file No. 01-072-1012 are in good agreement [24]. The Scherrer's formula ($D = 0.9\lambda/\beta\cos\theta$) was used to determine the sample's crystallite size. Here λ is the wavelength of X-rays, β is the full width at half maximum and θ is the Bragg's angle. The sample's nanoparticles were found to have an average crys-

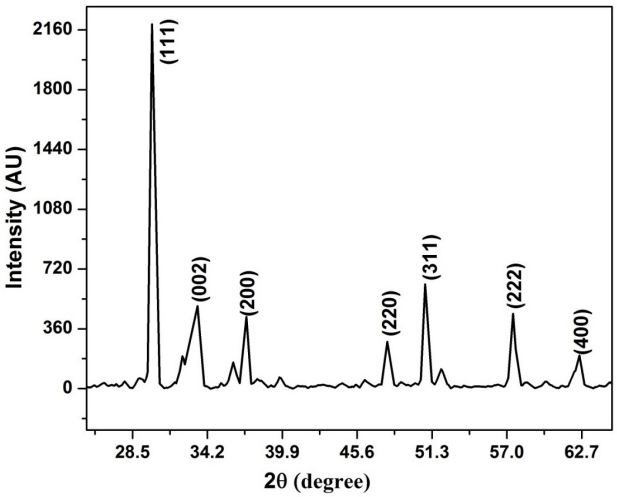

Figure 2. Powder XRD pattern of tin-added MnS nanomaterial.

tallite size (D) of 26.437 nm. The microstrain is caused by the point defects, grain boundary, stacking faults etc and the value of strain (ε) can be found by relation $\varepsilon = \beta/4\tan\theta$. The estimated average value of microstrain for TMS nanomaterial is 7.137×10^{-3}. The dislocation density measures the number of dislocations in a unit volume of the material and it is determined by using the relation $\rho_d = 1/D^2$ where D is the crystallite size. The calculated value of dislocation density is 1.431×10^{15} m^{-2} and this value is large due nano-size of the particles in the sample.

3.2 SEM studies

The SEM image of tin-added MnS (TMS) nanomaterial is shown in Fig. 3, and it can be seen from the fig. that the majority of the sample's particles are flower-shaped and slightly agglomerated. The image also shows that supra-aggregates of nanoparticles have formed. The particle size distribution in the photograph shows that the range of the size of the particles is between 15 and 35 nm.

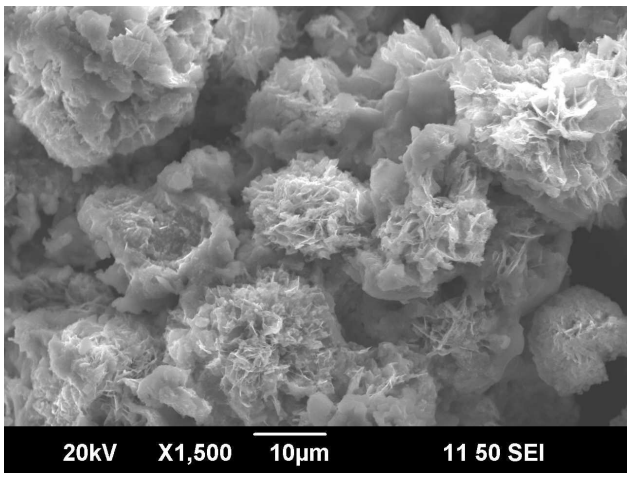

Figure 3. SEM image of TMS nanomaterial.

3.3 EDS studies

Analytical method like energy dispersive spectroscopy (EDS) is used to determine a sample's chemical or elemental makeup. It is an application of X-ray fluorescence spectroscopy that looks at how electromagnetic radiation and matter interact to reveal information about the sample. The detector for an EDS facility typically comprises of a lithium-drifted silicon device, and it is typically attached to a SEM equipment. A charge pulse proportional to the incident X-ray energy is produced when it strikes the detector. A charge-sensitive preamplifier transforms the charge pulse into a voltage pulse. The signal is then sent to a multichannel analyzer where the pulses are sorted by voltage. The energy determined from the voltage measurement for each incident X-ray is sent to a computer for display and further data evaluation [25, 26]. The EDS spectrum of tin-added MnS (TMS) nanomaterial was recorded using a Scanning Electron Microscope attached with EDS facility and it is shown in the Fig. 4. From the spectrum, it is ascertained that the elements such as Mn, S, Sn are mainly present in the sample and other additional elements like O, Na and Cl appear in the spectrum because reactants like tin chloride, sodium hydroxide, graph juice were used for preparation of the sample. The values of weight percentage of different elements present in TMS nanomaterial are provided in the Table 1.

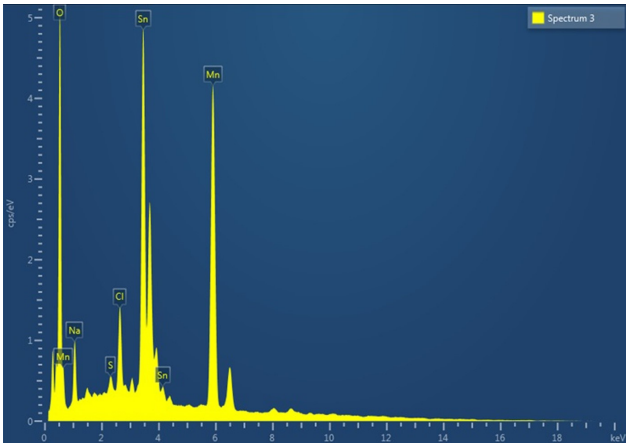

Figure 4. EDS spectrum of MnS:Sn nanomaterial.

Table 1. Weight percentage of elements in MnS:Sn nanomaterial.

Element	Weight (%)
Mn	27.21
Sn	23.44
S	47.27
Cl	1.45
O	2.37
Na	0.75

3.4 HRTEM and SAED studies

Transmission electron microscopes (TEM) make images by detecting the transmitted electrons from the sample, as opposed to scanning electron microscopes (SEM), which produce images by detecting the reflected electrons from

the sample's surface. As a result, TEM provides more internal data, including information on crystal structure, shape, and stress state. The TEM focuses an electron beam on the material to produce a highly detailed and magnified image. It is used to research nanostructured materials and its magnification power is more than 2 million times greater than that of a light microscope. The primary components of a TEM are an electron gun, an image-producing system, and an image-recording system, and they can be used to learn more about a nanoparticle's internal structure. The resolution of a high-resolution TEM (HRTEM) is greater than that of a TEM. While TEM has a resolution of 0.5 nm, HRTEM has a lattice resolution of 0.14 nm [27, 28]. Figs. 5 (a, b) displays the recorded HRTEM pictures of the TMS sample, while Fig. 6 displays the sample's SAED pattern. From the images, it is observed that there are spherical and elongated shaped nanoparticles and also there are agglomerations of particles in the prepared TMS nanomaterial. The particle sizes are estimated in the range of 18 to 25 nm. This value is close to that obtained by XRD studies. Each ring in the SAED pattern is filled with numerous white dots. From the spot pattern, it is deduced that nanoparticle is a single crystal and each spot on the ring indicates a crystal plane. A ring's spots all signify a collection of parallel planes with the same Miller indices. Thus, the (111), (200), (311) and (222) planes of the cubic crystal structure can be assigned to the four diffraction rings on the SAED pattern [29].

3.5 AFM study for TMS nanomaterial

The TMS sample was subjected to nanoparticle examination utilizing an atomic force microscope (AFM), which is regarded as one of the most well-liked scanning probe microscopes. In order to manipulate nanoparticles, the relationship between nanoparticles and the AFM probe was investigated. The size of the isolated nanoparticles may be easily calculated from the AFM picture by measuring the nanoparticle image height, as long as the substrate is flat [30, 31]. Measurements were made in an ambient environment, with an image resolution of 500 x 500 pixels and a scan speed of 1 to 5 m/s. The obtained 2-d and 3-d images for TMS nanomaterial are shown in the Fig. 7 (a, b, c). It is seen that there are white patches in AFM images and they are representing the dopant particles in the TMS sample [32].

3.6 Antimicrobial studies

Since their features are derived from their high area to volume ratio and high amount of surface atoms, nanomaterials have attracted a lot of attention recently. As the particles size shrinks, its accessible surface area increases, affecting the particle's characteristics. This feature makes nanoparticles wonderful and amazing materials for biomedical applications because many biological processes occur at the nanoscale level. Since viruses and bacteria are more likely to attack at the nanoscale, it is imperative to examine the antibacterial activity of the nanomaterials [33–35]. Five bacterial strains, including *Klebsiella pneumonia*, *Streptococcus*, *Staphylococcus aureus*, *Pseudomonas aeruginosa*, and *E. Coli*, were employed in this work to examine the antibacterial activity of TMS nanomaterial. The bacterial strains were sub-cultured in nutrient agar medium and the composition of the medium consists of (g/L): glucose - 0.5 g; yeast extract - 0.1 g; peptone - 0.25 g; KH_2PO_4 - 0.05 g; $MgSO_4$ - 0.01 g and NaCl - 1.0 g. The medium pH was adjusted to 7.0 by using HCl/NaOH. Then the isolates were inoculated individually and incubated at 37 °C for 24 h. Experiment was carried out in 100 mL Erlenmeyer flasks containing 50 mL of the culture medium and incubated for 1 day. The culture medium was poured into Petri dishes under sterile condition. Antibacterial activity against the bacterial strains was assessed and the diameter of the zone of inhibition was measured in mm. Five different bacterial strains were tested for antibacterial activity for the standard solution and the produced TMS nanomaterial. In the Figs. 8: (a) *Klebsiella pneumonia*, (b) *Streptococcus*, (c) *Staphylococcus aureus*, (d) *Pseudomonas aeruginosa*, and

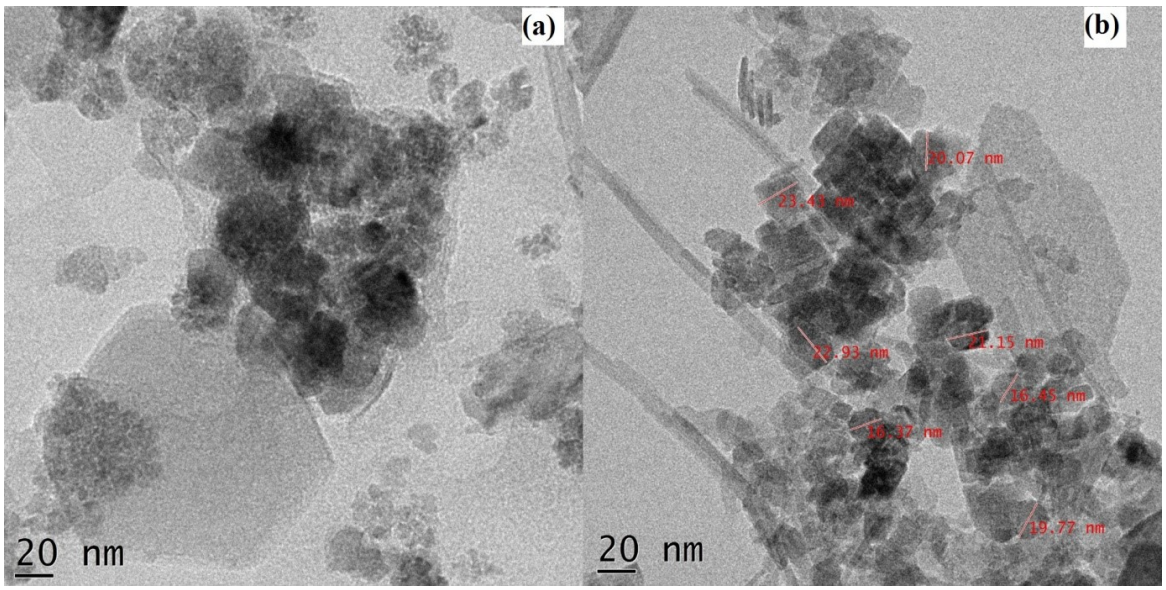

Figure 5. HRTEM images of TMS nanomaterial.

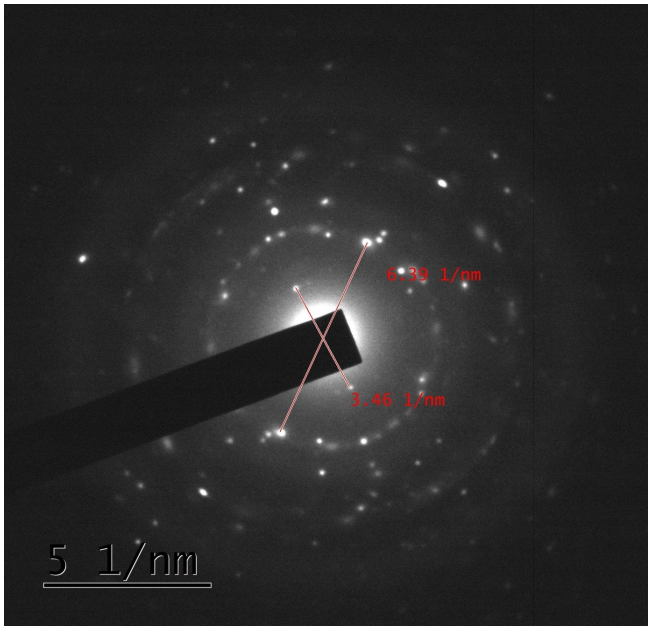

Figure 6. SAED pattern of TMS nanomaterial.

(e) *E. Coli*, photos related to a study on antibacterial activity are displayed. These images were used to quantify the diameter of the zone of inhibition, and the zone of inhibition measurement results are shown in Table 2. According to the results of Table 2, TMS nanomaterial has high antibacterial activity against the three pathogens *Klebsiella pneumonia*, *Escherichia coli*, and *Streptococcus* because its zone of inhibition values are comparable to those of the standard solution.

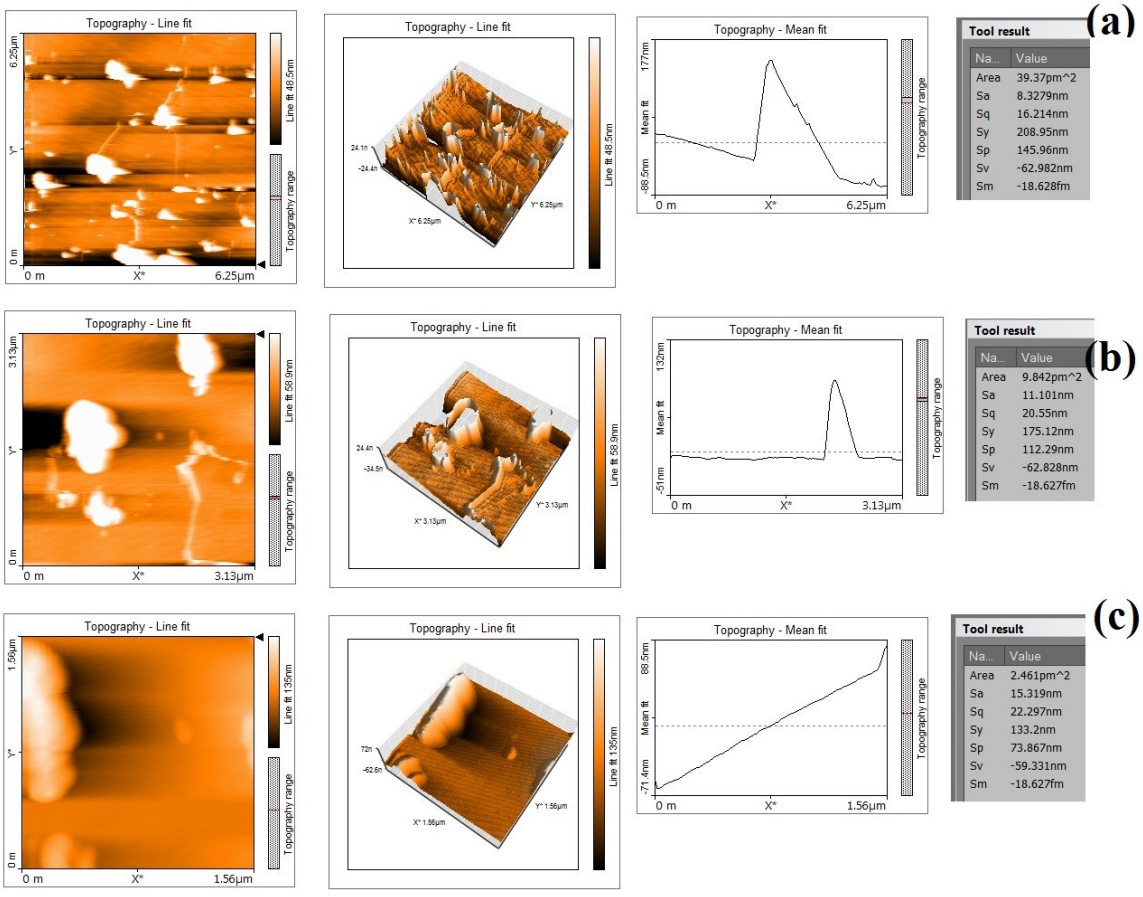

Figure 7. AFM images for TMS sample deposited on a substrate.

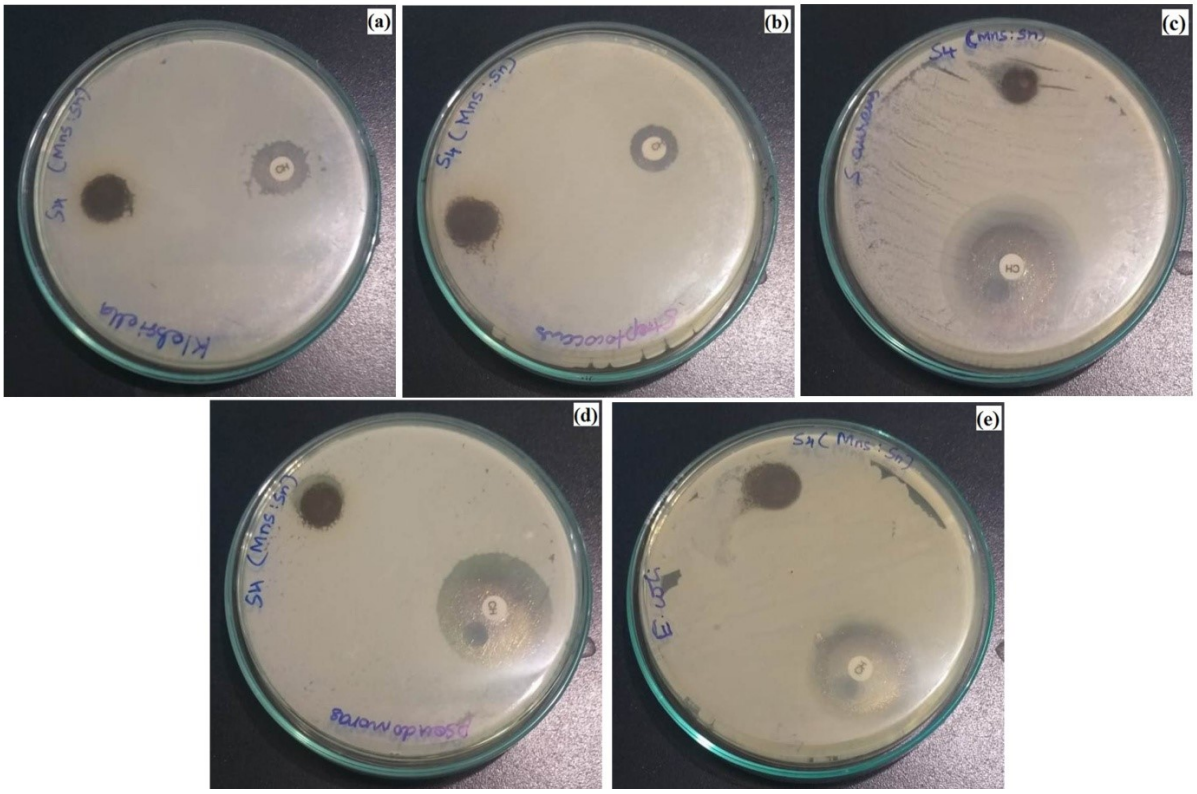

Figure 8. Photographs in connection with antibacterial activity for TMS nanomaterial against bacteria samples of a) *Klebsiella pneumonia*, b) *Streptococcus*, c) *Staphylococcus aureus*, d) *Pseudomonas aeruginosa* and e) *E. Coli*.

3.7 FTIR studies

The presence of functional groups of the as-prepared MnS: Sn nanoparticles synthesized by the present microwave-assisted solution method are analyzed using FTIR spectroscopy. The FTIR spectrum of the nanoparticles of tin-doped MnS is shown in Fig. 9. The broad absorption band located around 3420 cm^{-1} corresponds to the O-H stretching vibration of residual water and hydroxyl groups, while the absorption bands at 1620 cm^{-1} and 1460 cm^{-1} are due to the scissor bending mode of associated water. The band at 1153 cm^{-1} can be attributed to C-O stretching vibration.

3.8 UV-visible spectral studies

UV-visible spectroscopy is used to investigate absorption, transmittance, reflectance, optical band gap, and other linear optical constants. Fig. 10 displays the spectrum. The main characteristics of an absorption band are its position and intensity. The wavelength of radiation that has the same energy as an electronic transition determines the position of an absorption band. This spectroscopy has made it possible to monitor the band gap and absorption characteristics of nanoparticles. The sample absorbs less in the visible spectrum than in the UV spectrum, with the largest absorption occurring at $\lambda = 362$ nm. Using the formula $E_g = 1240/\lambda$, the band gap of TMS nanomaterial is determined to be 3.42 eV. Beyond 1850 nm, the absorbance increases slightly with increasing wavelength, contrary to the infrared portion of the spectrum where absorption is observed to be decreasing with increasing wavelength. Since absorbance is determined by the relationship $A = \log_{10}(1/T)$, where T is the transmittance, the transmittance spectrum of TMS nanomaterial is shown in Fig. 11 and exhibits the opposite behaviour of the absorbance spectrum. This graph shows that transmittance values are low in the UV and visible spectrums and

Table 2. Values of zone of inhibition for TMS nanomaterial against five bacterial strains.

Bacteria	Zone of inhibition (mm)	
	S4 (Mns:Sn)	Standard
Streptococcus aureus	15	25
Streptococcus	12	15
Klebsiella pneumonia	15	15
Pseudomonas aeruginosa	18	30
Escherichia coli	18	30

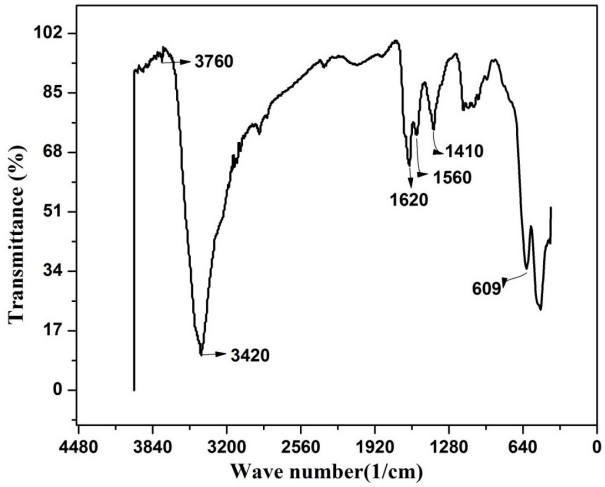

Figure 9. FTIR spectrum of the prepared MnS:Sn nanoparticles.

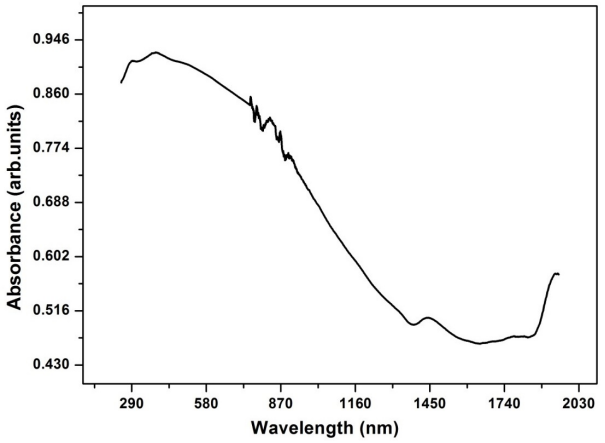

Figure 10. Absorbance spectrum of TMS nanomaterial.

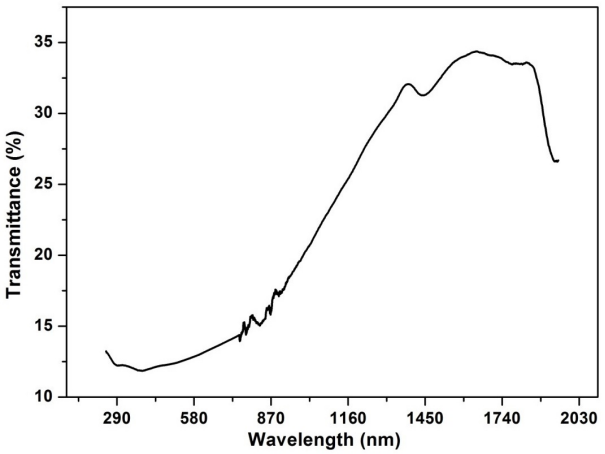

Figure 11. Transmittance spectrum of TMS nanomaterial.

high in the infrared spectrum [36, 37]. The linear refractive index of the TMS nanosample was calculated using the UV-visible spectral data and the relation used to determine the refractive index is $n = (1/T) + [(1/T) - 1]$ where T is the transmittance value. Fig. 12 shows the sample's refractive index change with photon energy. According to the findings, the TMS nanomaterial's refractive index (dispersed in acetone) marginally falls in the infrared region before rising when photon energy rises in the same region. Refractive index rises in the visible range and slightly falls in the UV range. Using the following relation, the sample's extinction coefficient (K) was calculated.

$$K = \frac{\alpha\lambda}{4\pi} \tag{1}$$

where α is the linear absorption coefficient, and λ is the light's wavelength. A graph is plotted between optical energy and extinction coefficient for TMS nanomaterial is shown in the Fig. 13. From the results, it is observed that the extinction coefficient decreases with increase in photon energy. The synthesized TMS nanomaterial has a low attenuation coefficient of the order of 10^{-5}, which suggests a weak interaction between photons and electrons [38–40]. The complex dielectric constant of the sample is written as

$$\varepsilon^* = \varepsilon_r + j\varepsilon_i = (n + jK)^2 \tag{2}$$

where ε_r is the real part of dielectric constant, ε_i is the imaginary part of dielectric constant, n is refractive index and K is the extinction coefficient. The above relation can be written as

$$\varepsilon^* = \varepsilon_r + j\varepsilon_i = n^2 - K^2 + j2nK \tag{3}$$

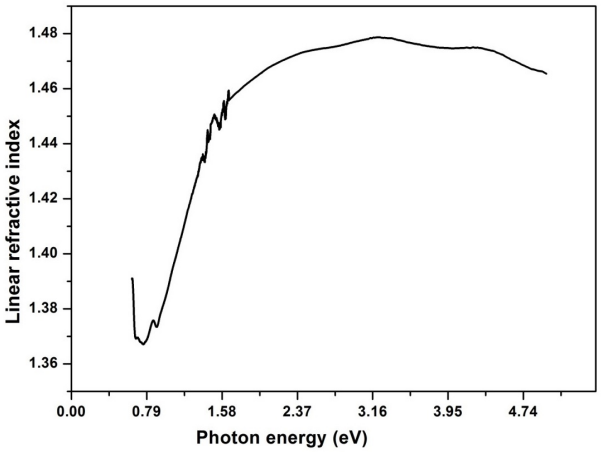

Figure 12. Variation of refractive index with photon energy for TMS nanomaterial.

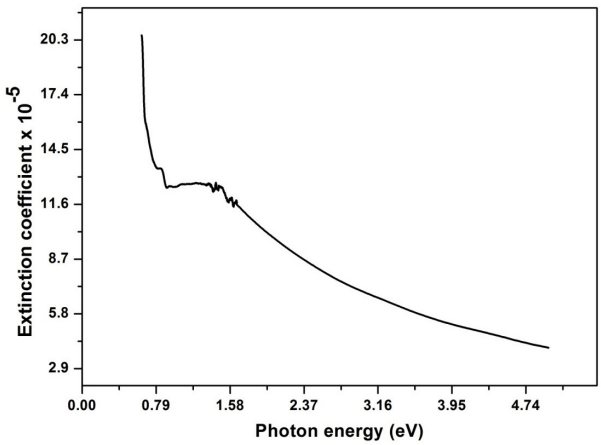

Figure 13. Variation of extinction coefficient with photon energy for TMS nanomaterial.

And hence the real and imaginary parts of dielectric constant can be written as

$$\varepsilon_r = n^2 - K^2 \text{ and } \varepsilon_i = 2nK \quad (4)$$

Using the aforementioned relations, the real and imaginary parts of the TMS material's dielectric constant were calculated [41]. For TMS nanomaterial, graphs of the real and imaginary parts of the dielectric constant as functions of wavelength are shown in Fig. 14. The obtained results demonstrate that as the wavelength grows, the real part reduces and the imaginary part increases. The sample is made of a high-quality material because of the sample's low imaginary part of dielectric constant value.

A parameter used to determine a material's optical qualities is its optical conductivity, which is computed in SI units using the formula given in equation [42].

$$\sigma_{op} = \varepsilon_0 cn\alpha \quad (5)$$

where c represents the velocity of light in free space, α is the absorption coefficient, ε_0 is the permittivity of free space or vacuum and n is the refractive index. The variation of optical conductivity with wavelength for TMS nanomaterial is shown in the Fig. 15. From the results, it can be seen that the sample's optical conductivity is highest in the UV region and that it decreases with increasing wavelength in the visible and near infrared regions while slightly increasing in the far infrared region.

3.9 Fluorescence studies

When exposed to visible or ultraviolet light, many samples not only absorb the light but also re-emit it at a different wavelength. Fluorescence is an effect that can be used to distinguish between different substances and determine their exact composition. Thus, fluorescence spectroscopy is a method of investigation that relies on a substance's ability to emit light rather than its propensity to absorb a particular wavelength of light. In this instance, the utilisation of light for excitation is referred to as photoluminescence. All directions receive the emission of the fluorescent light. As excitation sources, a variety of light sources, including lasers, may be employed. The light source for this experiment is a xenon arc lamp, which has a continuous

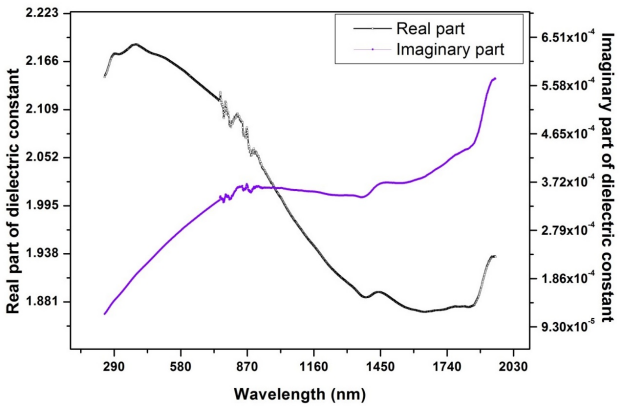

Figure 14. Plots of Real part of dielectric constant or imaginary part of dielectric constant with photon energy for TMS nanomaterial.

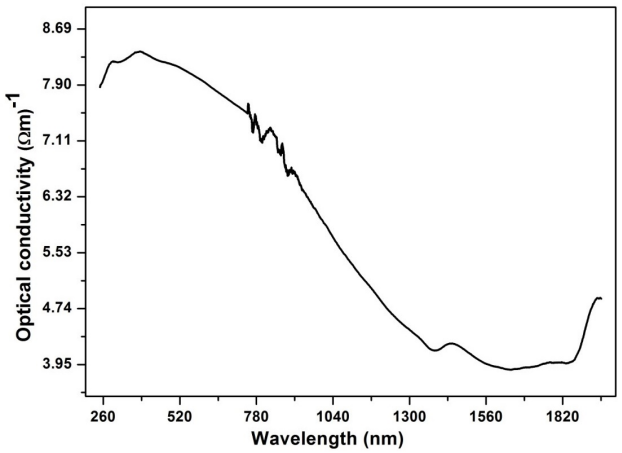

Figure 15. Variation of optical conductivity with wavelength for TMS nanomaterial.

emission spectrum and virtually constant intensity. The experiment's excitation wavelength is 240 nm. It is necessary to maintain a consistent excitation light wavelength when measuring the fluorescence spectrum. Biochemical, medicinal, and nanomaterial emission properties are investigated using photoluminescence spectroscopy [43]. Fig. 16 depicts the emission spectra of tin-doped MnS (TMS) nanomaterial. The emission peaks in the spectrum are located at wavelengths of 363 nm, 377 nm, 441 nm, 492 nm, 520 nm, 541 nm, and 593 nm. Among these peaks, 363 nm and 377 nm emission peaks belong to UV region and 441 nm, 492 nm, 520 nm, 541 nm and 593 nm peaks belong to visible region of the electromagnetic spectrum. Thus, TMS nanomaterial is an important UV and visible light emitting material when it is excited with 240 nm.

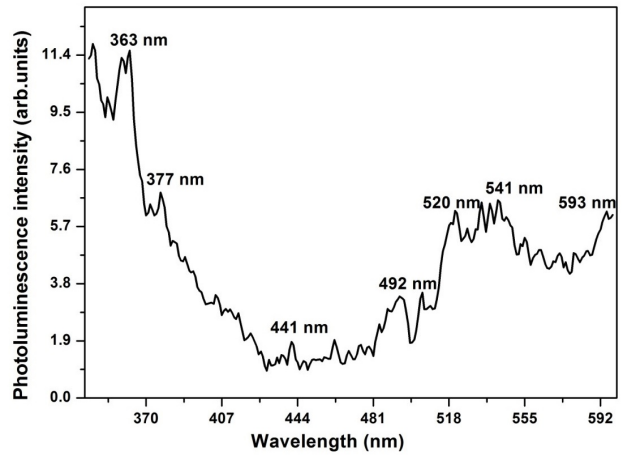

Figure 16. Photoluminescence spectrum of TMS nanomaterial.

3.10 TG/DTA studies

Fig. 17 displays the recorded TG/DTA curves of the TMS sample, which can be used to analyze the sample's thermal stability. A three-step breakdown process is depicted by the TG curve. Below 100 °C, the first stage can be seen with a weight loss of about 10% caused by the elimination of water that has been absorbed. The sample decomposes in the second step at a temperature of 500 °C. The emission of

gaseous particles from the sample causes the third stage of breakdown at 500 °C, and in this instance the DTA curve displays the broad exothermic peak. The material is melting and decomposing, causing the peaks at 300 °C and 500 °C. Hence, TG/DTA studies show that tin-doped MnS sample has high decomposition point.

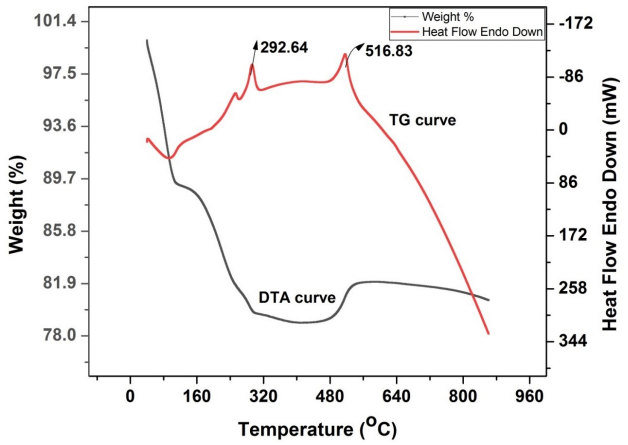

Figure 17. TG/DTA thermograms for TMS nanomaterial.

3.11 Cyclic voltammetric studies

The working electrode, reference electrode, and counter electrode are the three electrodes that make up a cyclic voltammetric (CV) device. Between the working electrode and the counter electrode, the potential is measured, and between the working electrode and the reference electrode, the current is measured. By putting the solution in contact with the working electrode surface and then making the electrode surface sufficiently positive or negative in voltage to compel electron transfer, the solution component is electrolyzed (oxidized or reduced) in this experiment. In CV, the working electrode's potential is swept across a potential range at a consistent pace while the resulting current is measured. This technique is utilized to get the peak current, peak potential, and distinctive voltammograms. Figs. 18 (a, b) show the cyclic voltammograms that correspond to the measurements of the current fluctuation with potential TMS nanomaterial at various scan speeds, including 0.05 V/s and 0.1 V/s. According to the findings, the peak current is higher for 0.1 V/s scan rates than for 0.05 V/s scan rates. The TMS sample exhibits a full cycle of voltammograms for both scan rates, indicating that the sample provides a full cycle of electrochemical reaction [44, 45].

3.12 Impedance studies

Impedance is a crucial factor used to describe the samples' electrical characteristics. The total resistance a device or circuit offers to the passage of an alternating current (AC) at a specific frequency is known as impedance (Z). A system's A.C. response to a sinusoidal disturbance is analyzed using an impedance analyzer, and the impedance is then calculated as a function of the perturbation's frequency. The real and imaginary components of impedance are denoted by Z' and Z'', respectively, in the complex impedance formula $Z^* = Z' - jZ''$ where Z' and Z'' are the real and imaginary

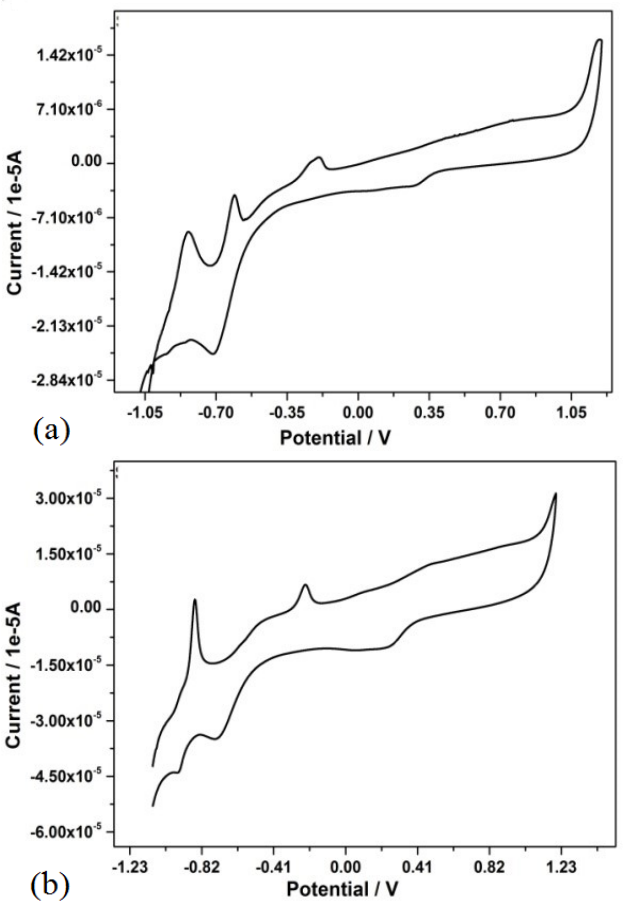

Figure 18. Plots of current versus potential at different scan rates like (a) 0.05 V/s and (b) 0.1 V/s for TMS nanomaterial.

components of impedance. The sum of a single RC circuit with parallel combination can be used to demonstrate the complex impedance of an electrode/insulator/electrode capacitor. The TMS preparation sample was formed into pellets with a 10 mm diameter and 2 mm thickness. A high-quality graphite paste was applied to the pellet's surfaces that came into contact with the electrodes. This experimental setup was protected from electricity and put in an electric oven to change the temperature. In order to measure the sample's real part and imaginary part of impedance, the electrodes of the experimental cell were linked to an impedance analyzer (IM 6 ZAHNER, Germany) for measuring the real part and imaginary part of impedance of the sample and the measurement was carried out at different frequency values and at 30 °C and 50 °C. The frequency-dependent real (Z') and imaginary (Z'') component impedance of TMS nanomaterial is shown in Figs. 19 and 20. The figs' values of Z' appear to converge more frequently. The findings indicate that impedance values are higher at 30 °C and lower at 50 °C. Additionally, when temperature increases, the peak widens, indicating the presence of an electrical relaxation mechanism. TMS nanomaterial's crystalline boundary resistance values are 1×10^5 Ω and 2.4×10^4 Ω at 30 °C and 50 °C, respectively. As a result, this sample has a negative temperature coefficient of resistance, indicating semiconducting or insulating behaviour [46, 47].

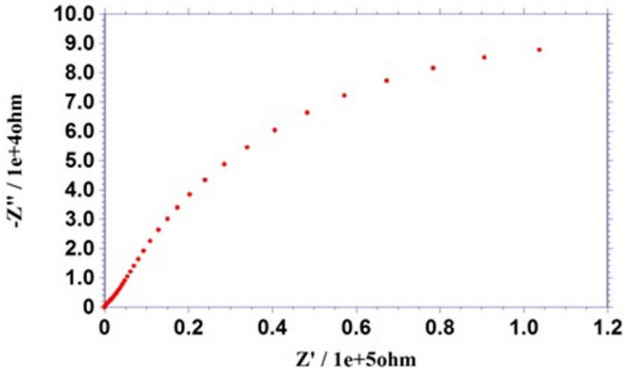

Figure 19. Impedance curve for TMS nanomaterial at 30 °C.

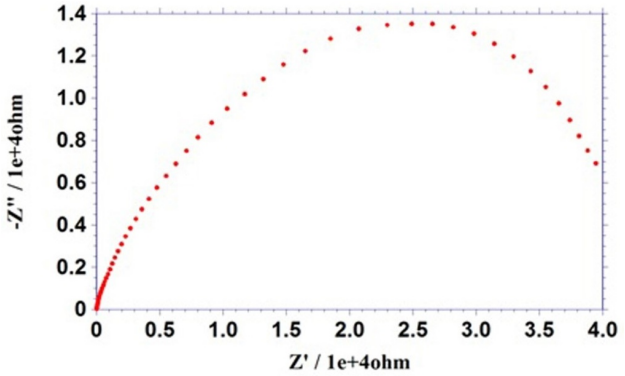

Figure 20. Impedance curve for TMS nanomaterial at 50 °C.

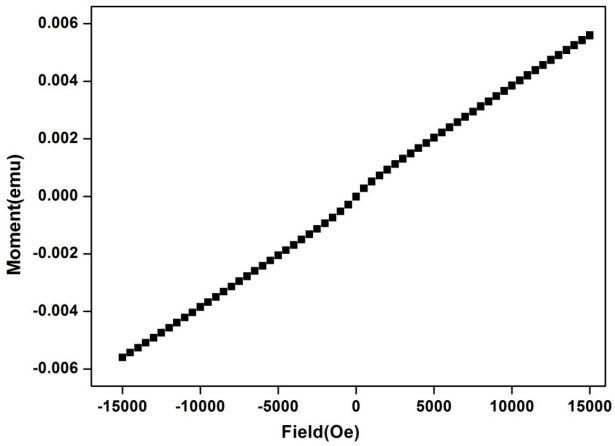

Figure 21. Hysteresis curve for TMS nanomaterial.

Table 3. Magnetic parameters of TMS nanomaterial.

Magnetic properties	Values
Saturation magnetization (M_s)	5.604×10^{-3} emu
Remanence magnetization (M_r)	7.755×10^{-6} emu
Squareness ratio (M_r/M_s)	0.00138

3.13 VSM studies

The magnetic characteristics of sample are determined using a vibrating sample magnetometer (VSM) instrument. Due to a change in the sample's magnetic field brought on by the vibrating component, a coil using Faraday's law of induction produces an electrical field. The sample is placed inside the sensing coils and the vibrating sample is caused to undergo mechanical vibration if it is exposed to a uniform magnetic field H, which will induce magnetization M in the sample and in the VSM. Once the vibration starts, a magnetic field forms around the sample, and as variations in the time of movement take place, the magnetization of the sample can be examined. Because changes in magnetic flux produce a voltage in the detecting coils that is proportional to the sample's magnetization [48]. At IIT Madras, a VSM investigation was conducted on TMS nanomaterial, and the resulting hysteresis curve is displayed in Fig.21. The values of the TMS nanomaterial's saturation magnetization (M_s), remanent magnetization (M_r), and squareness ratio are provided in Table 3. The findings show that the TMS sample falls under the category of paramagnetic material. The squareness ratio (M_r/M_s) was calculated, and the low value of M_r/M_s indicates that the crystalline of the sample are subject to magneto-static interaction.

4. Conclusion

Tin-doped MnS (TMS) nanomaterial was created using green synthesis, and various characterization tests were performed on it. The powder XRD technique revealed that the TMS nanomaterial's average particle size was 26.437 nm. A SEM analysis of TMS nanomaterial revealed the presence of agglomerated particles in the form of flowers. When the TMS nanomaterial's EDAX or EDS spectra was recorded, it was discovered that Mn, S, Sn, O, Na, and Cl were present. It can be seen that the TMS sample contains spherical and elongated-shaped nanoparticles from the HRTEM pictures that were captured. The Miller indices (111), (200), (311) and (222) have been assigned to the diffraction rings on the SAED pattern of the TMS sample. It has been determined that the white patches in the AFM photos are dopant particles in the manufactured TMS sample, which was dispersed in acetone and submitted to the AFM research. Five microorganisms, including *Staphylococcus aureus*, *Streptococcus*, *Klebsiella pneumonia*, *E. coli*, and *Pseudomonas aeruginosa*, were used in the antibacterial activity analysis of the TMS sample. For the TMS sample, an FTIR research was used to do functional group analysis. For TMS nanomaterial, UV-visible spectrum experiments were conducted, and numerous optical characteristics were identified and analyzed. When TMS sample was activated with UV light of 240 nm, it is seen from the fluorescence spectra that there are numerous emission peaks at 363 nm, 377 nm, 441 nm, 492 nm, 520 nm, 541 nm, and 593 nm. For the TMS sample, the TG/DTA thermal curves exhibit two peaks at 300 °C and 500 °C, which are caused by the sample's melting and disintegration. According to cyclic voltammetric analysis, the peak current is higher for 0.1 V/s scan rates than for 0.05 V/s. From the hysteresis curve, the values of saturation magnetization, remanent magnetization and squareness ratio of TMS nanomaterial were evaluated and it is concluded that TMS belongs to the category of paramagnetic material. Since this sample has the interesting

optical, magnetic and antibacterial properties, it could be useful in various fields like optoelectronics, solar energy conversion, fluorescence, and photocatalytic applications.

Acknowledgement
The authors are thankful to the staff members of Cochin University (Cochin), NIT (Trichy), St. Joseph's College (Trichy), IIT (Madras), VOC college (Tuticorin), Algappa University (Karaikudi) and IIT(Madras), for helping us to carry out the research work.

Authors contributions
Authors have contributed equally in preparing and writing the manuscript.

Availability of data and materials
The data that support the findings of this study are available from the corresponding author, upon reasonable request.

Conflict of interests
The authors assert that they do not have any identifiable conflicting financial interests or personal relationships that might be perceived to influence the work presented in this paper.

References

[1] S. Chavda, N. Limbasiya, P. Vamja, A. Vaishnani, K. Vachhani, B. Hirpara, M. Kandoliya, K. Gadani, D. Dhruv, A. D. Joshi, P. S. Solanki, and Shah N. A. "Studies on optical and electrical properties of CdO/Al_2O_3 composites.". *J. Sol-Gel Sci. Technol.*, 104:169–177, 2022.
DOI: https://doi.org/10.1007/s10971-022-05921-x.

[2] A. Zankat, K. Gadani, V. Vadgama, B. Udeshi, M. Gal, S. Solanki, A. Vaishnani, V. G. Shrimali, P. S. Solanki, N. A. Shah, and D. D. Pandya. "Frequency and temperature dependent electrical properties of ZnO–SnO_2 nanocomposites.". *Physica B.*, 617:413140, 2021.
DOI: https://doi.org/10.1016/j.physb.2021.413140.

[3] A. Zankat, K. Gadani, B. Rajyaguru, V. G. Shrimali, J. Joseph, H. Makwana, R. K. Trivedi, P. S. Solanki, N. A. Shah, and D. D. Pandya. "Structural and electrical properties of sol–gel grown (1 - x) (ZnO) + (x) (SnO_2) (x = 0, 0.25, 0.5) nanocomposites.". *J. Sol-Gel Sci. Technol.*, 99:198–210, 2013.
DOI: https://doi.org/10.1007/s10971-021-05544-8.

[4] B. Sadeghi, Sh. Ghammamy, Z. Gholipour, M. Ghorchibeigy, and A. Amini Nia. "Gold/hydroxypropyl cellulose hybrid nanocomposite constructed with more complete coverage of gold nano-shell.". *Micro Nano Lett.*, 6:209–213, 2011.
DOI: https://doi.org/10.1049/mnl.2011.0036.

[5] A. Amininia, K. Pourshamsian, and B. Sadeghi. "Nano-ZnO Impregnated on Starch-A Highly Efficient Heterogeneous Bio-Based Catalyst for One-Pot Synthesis of Pyranopyrimidinone and Xanthene Derivatives as Potential Antibacterial Agents.". *Russ. J. Org. Chem.*, 56:1279–1288, 2020.
DOI: https://doi.org/10.1134/S1070428020070234.

[6] N. Hebalkar, A. Lobo, S. R. Sainkar, S. D. Pradhan, W. Vogel, J. Urban, and S. K. Kulkarni. "Properties of zinc sulphide nanoparticles stabilized in silica.". *J. Mater. Sci.*, 36:4377–4384, 2001.
DOI: https://doi.org/10.1023/A:1017910131081.

[7] N. Rashmi Saragur, K. Chandrashekar Hosur, and A. Sangamesha Madanahalli. "Surface, structural and optical investigation on Poly Vinyl Alcohol (PVA)/Bi_2WO_6 nanocomposite films.". *Int. J. Nano Dimens.*, 13:267–281, 2024.
DOI: https://doi.org/10.22034/ijnd.2022.1946867.2109.

[8] B. Sadeghi and S. Ghammami. "Oxidation of Alcohols with Tetramethylammonium Fluorochromate in Aceticoi Acid.". *Russ. J. Gen. Chem.*, 75:1886–1888, 2005.
DOI: https://doi.org/10.1007/s11176-006-0008-0.

[9] Q. Wang, Y. Xu, X. Zhao, Y. Chang, Y. Liu, L. Jiang, J. Sharma, D. K. Seo, and H. Yan. "Facile one-step in situ functionalization of quantum dots with preserved photoluminescence for bioconjugation.". *J. Am. Chem. Soc.*, 129(20):6380–6381, 2007.
DOI: https://doi.org/10.1021/ja071434y.

[10] J. H. Joo, B. Na, T. Yu, J. H. Yu, Y. W. Kim, F. Wu, J. Z. Zhang, and T. Hyeon. "Generalized and facile synthesis of semiconducting metal sulfide nanocrystals. ". *J. Am. Chem. Soc.*, 125:11100–11105, 2003.
DOI: https://doi.org/10.1021/ja0357902.

[11] A. Puglisi, S. Mondini, S. Cenedese, A. M. Ferretti, N. Santo, and A. Ponti. "Monodisperse Octahedral α-MnS and MnO Nanoparticles by the Decomposition of Manganese Oleate in the Presence of Sulfur.". *Chem. Mater.*, 22:2804–2813, 2010.
DOI: https://doi.org/10.1021/cm903735e.

[12] Q. Tian, M. Tang, F. Jiang, Y. Liu, J. Wu, R. Zou, Y. Sun, Z. Chen, R. Li, and J. Hu. "Large-scaled star-shaped α-MnS nanocrystals with novel magnetic properties.". *Chem. Commun.*, 47:8100–8102, 2011.
DOI: https://doi.org/10.1039/C1CC11621E.

[13] D. S. Wang, W. Zheng, C. H. Hao, Q. Peng, and Y. D. Li. "A Synthetic Method for Transition-Metal Chalcogenide Nanocrystals.". *Chem. Eur. J.*, 15:1870–1875, 2009.
DOI: https://doi.org/10.1002/chem.200801815.

[14] H. Weller. "Quantized semiconductor particles: A novel state of matter for materials science.". *Adv. Mater.*, 5:88–95, 1993.
DOI: https://doi.org/10.1002/adma.19930050204.

[15] A. Kumar, A. Jakhmola, and V. Chaudhary. "Synthesis and photophysics of colloidal ZnS/PbS/ZnS nanocomposites—An analysis of dynamics of charge carriers.". *J. Photochem. Photobiol. A.*, 208: 195–202, 2009.
DOI: https://doi.org/10.1016/j.jphotochem.2009.09.015.

[16] D. Wang, Y. Cao, X. Zhang, X. Qian, X. Ai, Z. Liu, F. Liu, D. Wang, Y. Bai, T. Li, and X. Tang. "Synthesis and characteristics of ZnS/CdS composite nanocrystals in block copolymer micelle.". *J. Mater. Res.*, 14:2381–2384, 1999.
DOI: https://doi.org/10.1557/JMR.1999.0319.

[17] N. Kanabar, K. Gadani, V. G. Shrimali, K. Sagapariya, K. N. Rathod, B. Udeshi, J. Joseph, D. D. Pandya, P. S. Solanki, and N. A. Shah. "Structural and electrical properties of sol–gel grown nanostructured ZnO and $LaMnO_3$ particle-based nanocomposites.". *Appl. Phys. A.*, 127:122, 2021.
DOI: https://doi.org/10.1007/s00339-020-04243-5.

[18] M. Lagariya, M. Modi, H. Dadhich, M. Gal, K. Gadani, P. S. Solanki, and N. A. Shah. "Studies on structural and electrical behaviors of chemically grown ZnO/SnO_2 nanocomposites.". *Physica B.*, 577: 411774, 2020.
DOI: https://doi.org/10.1016/j.physb.2019.411774.

[19] J. Zheng, W. Ji, X. Wang, M. Ikezawa, P. Jing, X. Liu, H. Li, J. Zhao, and J. Masumoto. "Improved Photoluminescence of Mn-S/ZnS Core/Shell Nanocrystals by Controlling Diffusion of Mn Ions into the ZnS Shell.". *J. Phys. Chem. C.*, 114:15331–15336, 2010.
DOI: https://doi.org/10.1021/jp104513k.

[20] M. S. Sadjadi, B. Sadeghi, and K. Zare. "Natural bond orbital (NBO) population analysis of cyclic thionylphosphazenes, [NSOX ($NPCl_2$)2]; X=F (1), X=Cl (2).". *J. Mol. Struct. THEOCHEM.*, 27-33:817, 2007.
DOI: https://doi.org/10.1016/j.theochem.2007.04.015.

[21] M. A. Ammulu, K. V. Viswanath, A. K. Giduturi, P. K. Vemuri, U. Mangamuri, and S. Poda. "Phytoassisted synthesis of magnesium oxide nanoparticles from Pterocarpus marsupium rox. b heartwood extract and its biomedical applications.". *J. Genet. Eng. Biotechnol.*, 19:1–18, 2021.
DOI: https://doi.org/10.1186/s43141-021-00119-0.

[22] S. Abinaya and P. K. Helen. "Magnesium Oxide Nanoparticles: Effective Antilarvicidal and Antibacterial Agents.". *ACS Omega.*, 8: 5225–5233, 2023.
DOI: https://doi.org/10.1021/acsomega.2c01450.

[23] M. A. Abdulaziz, D. M. Paul, A. Firoz, J. V. Inigo, F. S. W. George, T. Floriana, O. Paul, D. David, and J. L. David. "Structural Investigations of α-MnS Nanocrystals and Thin Films Synthesized from Manganese (II) Xanthates by Hot Injection, Solvent-Less Thermolysis, and Doctor Blade Routes.". *ACS Omega.*, 6:27716–27725, 2021.
DOI: https://doi.org/10.1021/acsomega.1c02907.

[24] T. Mazhar. "Bio-assisted synthesis of bi-metallic (Ag-Zn) nanoparticles by leaf extract of Azadirachta indica and its antimicrobial properties.". *Int. J. Nano Dimens.*, 13:168–178, 2024.
DOI: https://doi.org/10.22034/ijnd.2022.686558.

[25] M. Beiranvand, B. Ajerloo, and A. Mohammadi. "Low-cost and eco-friendly phyto-synthesis of Silver nanoparticles by using grapes fruit extract and study of antibacterial and catalytic effects.". *Int. J. Nano Dimens.*, 8:49–60, 2024.
DOI: https://doi.org/10.22034/ijnd.2017.24376.

[26] M. Yamamoto, Y. Kashiwagi, T. Sakata, H. Mori, and M. Nakamoto. "Synthesis and morphology of star-shaped gold nanoplates protected by poly (N-vinyl-2-pyrrolidone). ". *Chem. Mater.*, 17:5391–5393, 2005.
DOI: https://doi.org/10.1021/cm0515000.

[27] B. Ballarin, M. C. Cassani, D. Tonelli, E. Boanini, S. Albonetti, M. Blosi, and M. Gazzano. "Gold Nanoparticle-Containing Membranes from in Situ Reduction of a Gold (III)-Aminoethylimidazolium Aurate Salt.". *J. Phys. Chem. C.*, 114: 9693–9701, 2010.
DOI: https://doi.org/10.1021/jp1024262.

[28] A. M. Zardkhoshoui, B. Ameri, and S. S. H. Davarani. "α-MnS@Co_3S_4 hollow nanospheres assembled from nanosheets for hybrid supercapacitors.". *Chem. Eng. J.*, 422:129953, 2021.
DOI: https://doi.org/10.1016/j.cej.2021.129953.

[29] B. Roberto, P. Gian Bartolo, and R. Luigi. "AFM Measurements and Tip Characterization of Nanoparticles with Different Shapes.". *Nanomanuf. Metrol.*, 5:127–138, 2022.
DOI: https://doi.org/10.1007/s41871-022-00125-x.

[30] L. M. Lacava, B. M. Lacava, R. B. Azevedo, Z. G. M. Lacava, N. Buske, A. L. Tronconi, and P. C. Morais. "Nanoparticle sizing: A comparative study using atomic force microscopy, transmission electron microscopy, and ferromagnetic resonance.". *J. Mag. Mat.*, 225:79–83, 2001.
DOI: https://doi.org/10.1016/S0304-8853(00)01231-2.

[31] J. M. Daniel, C. D. Andra, L. G. Cristina, E. G. Hermann, H. Peter, H. Gerhard, J. D. Y. James, F. D. Yves, and A. David. "Atomic Force Microscopy-Based Force Spectroscopy and Multiparametric Imaging of Biomolecular and Cellular Systems.". *Chem. Rev.*, 121: 11701–11725, 10.

[32] C. Zhang, Z. Yi, and W. Xu. "Scanning probe microscopy in probing low-dimensional carbon-based nanostructures and nanomaterials.". *Mater. Futures.*, 1:032301, 2022.
DOI: https://doi.org/10.1088/2752-5724/ac8a63.

[33] S. J. Park, H. H. Park, S. Y. Kim, S. J. Kim, K. Woo, and G. P. Ko. "Antiviral properties of silver nanoparticles on a magnetic hybrid colloid.". *Appl. Environ. Microbiol.*, 80:2343–2350., 2014.
DOI: https://doi.org/10.1128/AEM.03427-13.

[34] A. H. Hashem, E. Saied, B. H. Amin, F. O. Alotibi, A. A. Al-Askar, A. A. Arishi, F. M. Elkady, and M. A. Elbahnasawy. "Antifungal Activity of Biosynthesized Silver Nanoparticles (AgNPs) against *Aspergilli* Causing Aspergillosis: Ultrastructure Study.". *J. Funct. Biomater.*, 13:242, 2016.
DOI: https://doi.org/10.3390/jfb13040242.

[35] A. Brandelli. "Nanocomposites and their application in antimicrobial packing.". *Front. Chem.*, 12, 2024.
DOI: https://doi.org/10.3389/fchem.2024.1356204.

[36] S. Karuppusamy, S. Muralidharan, B. K. Dinesh, P. Sakthivel, and C. Dongjin. "Thermal, dielectric, mechanical and structural behavior of 2-amino 4-methylpyridinium 4-nitrophenolate 4-nitrophenol bulk single crystal.". *Heliyon*, 9:e18260, 2023.
DOI: https://doi.org/10.1016/j.heliyon.2023.e18260.

[37] T. N. Steven, J. R. Kevin, I. Toshiko, and L. Xiaojun. "Characterization of Mass Transfer within the Crystal-Solution Boundary Layer of l-Alanine 120 Faces Using Laser Interferometry during Growth and Dissolution.". *Cryst. Growth Des.*, 23:2755–2769, 2023.
DOI: https://doi.org/10.1021/acs.cgd.2c01541.

[38] C. R. Raja, G. Gokila, and A. A. Joseph. "Growth and spectroscopic characterization of a new organic nonlinear optical crystal: L-Alaninium succinate.". *Spectrochim. Acta, Part A.*, 16:753–756, 2009.
DOI: https://doi.org/10.1016/j.saa.2008.11.030.

[39] L. Pei, J. Xiao, H. Menglin, K. Lei, C. Shiyou, G. Adam, and H. Bing. "Defect engineering of second-harmonic generation in nonlinear optical semiconductors.". *Cell Rep. Phys. Sci.*, 3:101111, 2022.
DOI: https://doi.org/10.1016/j.xcrp.2022.101111.

[40] D. Shanthi, P. Selvarajan, and S. Perumal. "Linear optical constants and photoluminescence characteristics of beta-alaninium picrate (BAP) crystals.". *Optik*, 127:3192–3199, 2016.
DOI: https://doi.org/10.1016/j.ijleo.2015.11.189.

[41] K. A. Aly. "Comment on the relationship between electrical and optical conductivity used in several recent papers published in the journal of materials science: materials in electronics. ". *J. Mater. Sci: Mater. Electron.*, 33:2889–2898, 2022.
DOI: https://doi.org/10.1007/s10854-021-07496-9.

[42] M. Zhar, G. A. Nowsherwan, M. A. Iqbal, S. Ikram, A. F. Butt, M. Khan, N. Ahmad, S. S. Hussain, M. A. Raza, J. R. Choi, S. Riaz, and S. Naseem. "Morphological, Photoluminescence, and Electrical Measurements of Rare-Earth Metal-Doped Cadmium Sulfide Thin Films.". *ACS Omega.*, 8:36321–36332, 2023.
DOI: https://doi.org/10.1021/acsomega.3c04936.

[43] G. Zlatic, A. Arapovic, I. Martinovic, A. Martinovic Bevanda, P. Boskovic, A. Prkic, A. Paut, and T. Vukusic. "Antioxidant Capacity of Herzegovinian Wildflowers Evaluated by UV–VIS and Cyclic Voltammetry Analysis.". *Molecules*, 27:5466, 2022.
DOI: https://doi.org/10.3390/molecules27175466.

[44] S. Singh, P. Narasimhappa, N. A. Khan, V. Chauhan, N. Shehata, S. K. Behera, J. Singh, and P. C. Ramamurthy. "Effective voltammetric tool for Nano-detection of triazine herbicide (1-Chloro-3-ethylamino-5-isopropylamino-2,4,6-triazine) by naphthalene derivative.". *Environ. Res.*, 236:116808, 2023.
DOI: https://doi.org/10.1016/j.envres.2023.116808.

[45] G. F. Da Silva, S. Martini, J. C. B. Moraes, and L. K. Teles. "AC impedance spectroscopy (AC-IS) analysis to characterize the effect of nanomaterials in cement-based mortars. ". *Construct. Build. Mater.*, 269:121260, 2021.
DOI: https://doi.org/10.1016/j.conbuildmat.2020.121260.

[46] M. Deep, S. Chandra Bhal, and S. Akhilesh Kumar. "Synthesis and characterization of BaTi1-xNbxO_3 ferroelectric perovskite oxides with tunable band gap, anomalous photovoltage, and enhanced energy storage.". *J. Mater. Sci.: Mater. Electron.*, 35:912, 2024.
DOI: https://doi.org/10.1007/s10854-024-12636-y.

[47] T. Balgovind, T. Babu, and R. N. P. Choudhary. "AC Impedance and Modulus Spectroscopic Studies of Pb($Zr_{0.35-x}$Ce$xTi_{0.65}$) O_3 (x = 0.00, 0.05, 0.10, 0.15) Ferroelectric Ceramics.". *Mater. Chem. Phys.*, 256:123655, 2020.
DOI: https://doi.org/10.1016/j.matchemphys.2020.123655.

[48] S. Foner. "The vibrating sample magnetometer: Experiences of a volunteer.". *J. Appl. Phys.*, 79:4740–4745, 1996.
DOI: https://doi.org/10.1063/1.361657.